frontiers in Materials

ORIGINAL RESEARCH
published: 05 July 2021
doi: 10.3389/fmats.2021.709757

The Verification of Thermoelectric Performance Obtained by High-Throughput Calculations: The Case of GeS_2 Monolayer From First-Principles Calculations

*Xiaolian Wang[1], Wei Feng[1], Chen Shen[2], Zhehao Sun[3], Hangbo Qi[2], Mao Yang[1], Yonghui Liu[1], Yuchen Wu[1] and Xiaoqiang Wu[1]**

[1]School of Mechanical Engineering, Chengdu University, Chengdu, China, [2]Institute of Materials Science, Technical University of Darmstadt, Darmstadt, Germany, [3]School of Energy and Power Engineering, Dalian University of Technology, Dalian, China

OPEN ACCESS

Edited by:
Guangzhao Qin,
Hunan University, China

Reviewed by:
Ning Wang,
University of Electronic Science and Technology of China, China
Lei Wang,
University of Science and Technology of China, China
Bingke Li,
Nanyang Institute of Technology, China

***Correspondence:**
Xiaoqiang Wu
wuxiaoqiang@cdu.edu.cn

Specialty section:
This article was submitted to Energy Materials, a section of the journal Frontiers in Materials

Received: 14 May 2021
Accepted: 01 June 2021
Published: 05 July 2021

Citation:
Wang X, Feng W, Shen C, Sun Z, Qi H, Yang M, Liu Y, Wu Y and Wu X (2021) The Verification of Thermoelectric Performance Obtained by High-Throughput Calculations: The Case of GeS_2 Monolayer From First-Principles Calculations. Front. Mater. 8:709757. doi: 10.3389/fmats.2021.709757

Electronic fitness function (EFF, achieved by the electrical transport properties) as a new quantity to estimate thermoelectric (TE) performance of semiconductor crystals is usually used for screening novel TE materials. In recent years, because of the high EFF values, an increasing number of two-dimensional materials have been predicted to have the potential for TE applications *via* high-throughput calculations. Among them, the GeS_2 monolayer has many interesting physical properties and is being used for industrial applications. Hence, in this work, we systematically investigated the TE performance, including both electronic and thermal transport properties, of the GeS_2 monolayer with first-principles calculations. The results show that the structure of the GeS_2 monolayer at 700 K is thermally unstable, so we study its TE performance only at 300 and 500 K. As compared with other typical TE monolayers, the GeS_2 monolayer exhibits excellent electronic transport properties but a relatively high lattice thermal conductivity of 5.71 $W m^{-1} K^{-1}$ at 500 K, and thus an unsatisfactory *ZT* value of 0.23. Such a low ZT value indicates that it is necessary to consider not only the electron transport properties but also the thermal transport properties to screen the thermoelectric materials with excellent performance through high-throughput calculations.

Keywords: GeS_2 monolayer, thermoelectric, transport property, high-throughput calculations, first-principles calculations

INTRODUCTION

In the past decades, the development of environment-friendly renewable energy has been the main task since it has alleviated the current global energy crisis and the greenhouse effect to some extent (Biswas et al., 2012; Wang and Wu, 2012; Tan et al., 2016). Thermoelectric (TE) materials, which are capable of converting waste heat into electricity directly and reversibly without air pollution, have attracted intense attention (Bell 2008; Wang et al., 2016; Wang et al., 2017). The conversion efficiency is characterized by a dimensionless figure of merit, $ZT = S^2 T\sigma/(\kappa_e + \kappa_l)$ (Snyder and Toberer, 2008), where the *S*, *T*, σ, κ_e, and κ_l represent the Seebeck coefficient, absolute temperature, electrical conductivity, and electronic and lattice thermal conductivity, respectively. However, it is extremely difficult to simultaneously increase the power factor *PF* ($S^2\sigma$) while reducing the thermal

conductivity $\kappa(\kappa_e + \kappa_l)$ due to the conflicting properties of TE materials. Therefore, improving the conversion efficiency of TE materials is a challenging and desirable task. Some semiconductors with great TE performance have been found so far. For example, a high *ZT* value of 2.6 ± 0.3 at 923 K in a promising thermoelectric material, SnSe single crystals, was reported due to the strong anharmonicity, and thus the exceptionally low lattice thermal conductivity (0.23 $W\,m^{-1}\,K^{-1}$) (Zhao et al., 2014). Besides, another promising candidate of TE materials, PbTe, exhibits a high *ZT* value above 1.5 at 773 K (Heremans et al., 2008). However, it is necessary to further improve their TE performance to achieve industrial applications. Therefore, some methods like doping (Liu et al., 2008), alloying (Row et al., 1981), and nanostructuring (Yuan et al., 2018) were reported to enhance the *ZT* value. Except for these approaches, screening new TE materials is also an effective strategy to improve the *ZT* value *via* experimental research (Nielsen et al., 2013; Tang et al., 2015; Li et al., 2018) and theoretical predictions [such as first-principles calculations (Wang et al., 2017; Ouyang et al., 2018) and high-throughput computations (Chen et al., 2016; Li M. et al., 2019; Li R. et al., 2019; Ortiz et al., 2019)].

High-throughput computations are usually used to screen high-performance functional materials according to their EFF (electronic fitness function) values, which is a new quantity to estimate TE performance of materials, such as $SnSe_2$ (Jia et al., 2020) and SnO (Miller et al., 2017). As a chalcogenide material, GeS_2 has interesting physical properties and is being used for industrial applications, such as photodetection (Yang et al., 2019), photoresistor, or antireflection coating (Málek and Shánělová, 1999). Especially, glassy germanium disulfide has been heavily studied for many years (Lucovsky et al., 1974; Tichý et al., 1982; Weinstein et al., 1982) and was still the subject of recent experimental investigations (Petri and Salmon, 2001). Besides, the 1T-CdI_2–type GeS_2 monolayer was recently reported to have potential as a promising TE material due to its highest peak EFF value (0.3×10^{-19} $W^{5/3}\,ms^{-1/3}\,K^{-2}$) for p-type carriers (Sarikurt et al., 2020). However, the high EFF value only reflects its strong electron transport performance, but the thermal transport property of the GeS_2 monolayer is not yet clear. Most importantly, there has not been a focus on the TE performance of GeS_2 monolayers that integrate electrical transport and thermal transport. Consequently, the further exploration of the electronic and thermal transport properties of the GeS_2 monolayer is quite reasonable and desirable.

In this work, the TE properties of two-dimensional (2D) isotropic GeS_2 are comprehensively studied based on first-principles calculations combined with the Boltzmann transport theory. The results show that this monolayer exhibits great electronic properties, for example, high *PF* value (3.4 $mW\,m^{-1}\,K^{-2}$) at 300 K, which is consistent with the high EFF values obtained with high-throughput computations. However, due to the unsatisfactory thermal transport properties, the *ZT* value of 2D GeS_2 can only reach 0.23 at 500 K. This study suggests that the GeS_2 monolayer has poor TE performance, thus proving that the method of predicting high-efficiency TE materials according to the EFF values obtained *via* high-throughput computations may be incomplete.

COMPUTATIONAL DETAILS

In this study, our first-principles calculations are performed by using density functional theory (DFT), as implemented in the Vienna *Ab initio* Simulation Package (VASP) (Kresse and Hafner, 1993; Kresse and Furthmüller, 1996a; Kresse and Furthmüller, 1996b). The generalized gradient approximation (GGA) (Perdew et al., 1996; Zhang et al., 2018) with Perdew–Burke–Ernzerhof (PBE) parametrization (Qiao et al., 2018) is applied as the exchange–correlation potential. For obtaining the accurate electronic structure, the Heyd–Scuseria–Ernzerhof hybrid functional (HSE06) (Heyd et al., 2003) is adopted to describe the exchange–correlation energy. The cutoff energy of 550 eV is set for the plane-wave basis, and the Brillouin zones are sampled with 15 × 15 × 1 Monkhorst–Pack special k-point meshes for 2D GeS_2. The convergence criteria for energy and force are 1×10^{-5} eV and 1×10^{-4} eV/Å, respectively, which is accurate enough and used in many studies (Sun et al., 2003). To avoid the effect of layer–layer interactions, a sufficiently large vacuum layer of 20 Å is constructed perpendicular to the layer plane in all the calculated structures.

In order to obtain κ_l, the second- and third-order interatomic force constants (IFCs) are calculated, first using the Phonopy code and the Thirdorder.py script, respectively (Togo et al., 2008; Li et al., 2014). Then κ_l can be derived from the mode-resolved phonon properties based on the obtained harmonic and anharmonic IFCs by solving the Boltzmann transport equation as implemented in the ShengBTE code (Li et al., 2014), which is expressed as follows:

$$\kappa_l = \frac{1}{k_B T^2 \Omega N} \sum_{\lambda} n_0 (n_0 + 1) (\hbar\omega_\lambda)^2 v_\lambda^\alpha v_\lambda^\beta \tau_\lambda, \quad (1)$$

where α and β are the Cartesian components of *x*, *y*, or *z*, and k_B, ħ, Ω, *N*, λ, n_0, ω_λ, τ_λ, and v_λ are the Boltzmann constant, Planck constant, volume of the unit cell, number of phonon wave vectors, phonon mode, Bose–Einstein distribution function, phonon frequency, phonon lifetime, and phonon group velocity, respectively. For calculating the accurate κ_l, the cutoff value and the Q-grid mesh are set to the 14th and 25 × 25 × 1, respectively.

The electronic transport properties are obtained by employing the Boltzmann transport equation combined with the relaxation time approximation (RTA) *via* the BoltzTraP2 code with a denser 31 × 31 × 1 k-point sampling (Madsen et al., 2018). Although RTA tends to overestimate power factors, because of computational convenience, we still adopt this approximation. It was also used in a study on the electronic transport properties of two-dimensional triphosphides (InP3, GaP3, SbP3, and SnP3) (Sun et al., 2020). The relaxation time τ is calculated using deformation potential (DP) theory combined with the effective

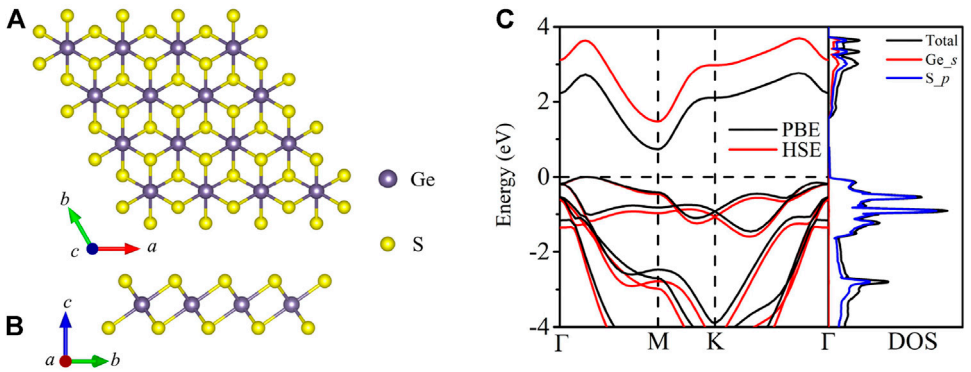

FIGURE 1 | Crystal structure of top views **(A)** and side view **(B)** for monolayer GeS_2. Electronic band structure and DOS (states/eV/u.c.) **(C)** for monolayer GeS_2.

mass approximation (Bardeen and Shockley, 1950) as shown below:

$$\tau = \frac{\mu m^*}{e} = \frac{2\hbar^3 C}{3k_B T m^* E_1^2}, \quad (2)$$

where $\hbar$, k_B, m^*, C, and E_1 are the Planck constant, Boltzmann constant, effective mass, elastic constant, and DP constant, respectively. For the electronic thermal conductivity κ_e, in this study, it is obtained using the Wiedemann–Franz law, that is, $\kappa_e = L\sigma T$ (Jonson and Mahan, 1980) Besides, κ_e can also be obtained directly from the BoltzTraP2 code, that is, $\kappa_e = \kappa_0 - T\sigma S^2$ (Madsen et al., 2018) A recent study put forward that the results which were obtained from the output of BoltzTraP and from using the Wiedemann–Franz law agree very well with each other (Li M. et al., 2019).

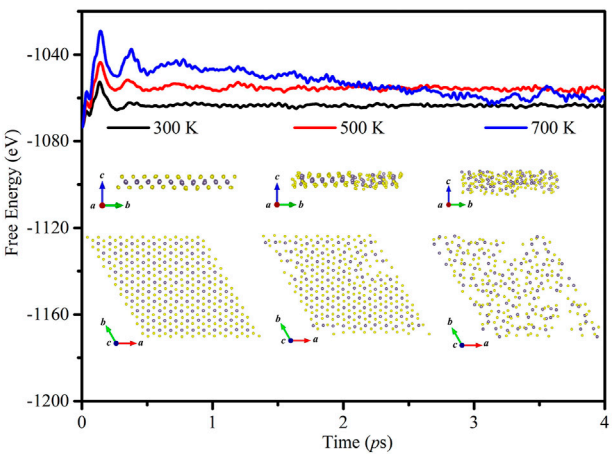

FIGURE 2 | Free energy fluctuations with respect to time in AIMD simulations and equilibrium structures for the GeS_2 monolayer obtained *via* AIMD simulations at 300, 500, and 700 K.

RESULTS AND DISCUSSION

Geometrical Characteristics and Electronic Structures

The optimized structure of 2D GeS_2 possesses a trigonal structure, with the $P\bar{3}$ m1 space group consisting of 1 Ge and 2 S atoms in the primitive unit cell, as shown in **Figures 1A, B**. The optimized lattice constants are $a = b = 3.45$ Å with the PBE method, which is consistent with the previous first-principles results, which are $a = b = 3.45$ Å (Sarikurt et al., 2020). Then based on the optimized structure, the electronic band structure and density of states (DOS) distributions are obtained by using the HSE06 functional near the Fermi level of the GeS_2 monolayer, and then we compare the band structures with the HSE06 and PBE functionals, and the results are given in **Figure 1C**. The calculated results show that an indirect bandgap of 1.47 eV with HSE06 is twice over that of 0.73 eV with PBE, which is large enough to overcome the bipolar conduction effect and thus avoid the decreasing of the Seebeck coefficient (Shi et al., 2015). As for DOS distribution, it is contributed by both *s* orbitals of the Ge atom and *p* orbitals of the S atoms near the CBM, and around the VBM, it is only dominated by the *p* orbitals of the S atoms.

Stability and Phonon Dispersion

To confirm the thermal stability of monolayer GeS_2, *ab initio* molecular dynamics (AIMD) simulations are performed between 300 and 700 K with a time period up to 4 *p*s. The results as given in **Figure 2** show that the average values of the total energy remain nearly constant after 1 *p*s at 300 and 500 K. However, the curve at 700 K still declines after 1 *p*s. Besides, the structures are well maintained and all the atoms in monolayer GeS_2 are vibrating around their equilibrium positions at 300 and 500 K, but the atom distribution is disordered at 700 K, which suggests that the structure is unstable at 700 K. Consequently, we choose 300 and 500 K as the typical temperatures to study the TE properties of the GeS_2 monolayer.

Next, we focus on the thermal properties of the GeS_2 monolayer and figure out the phonon spectrum and phonon DOS as given in **Figure 3** to confirm its dynamic stability. There are nine phonon branches found in the phonon dispersion since there are three atoms in the unit cell. Among them, the three

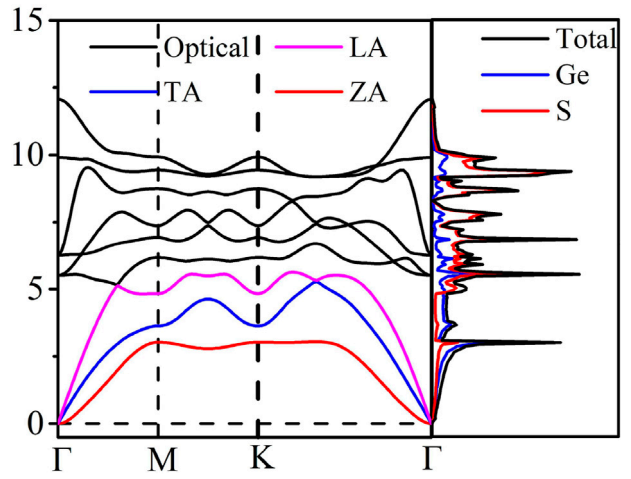

FIGURE 3 | Phonon dispersion and phonon DOS for monolayer GeS_2.

lowest vibration frequency branches are the out-of-plane flexural acoustic branch (ZA), the in-plane linear transverse acoustic branch (TA), and the longitudinal acoustic branch (LA), respectively. From **Figure 3**, one can see that no imaginary phonon branches are observed in the phonon dispersion, suggesting that the GeS_2 monolayer is dynamically stable. It is noted that there is no overlapped part among acoustic and optical branches, which suggests that the coupling effect of acoustic–acoustic modes and acoustic–optical modes is extremely weak. This phenomenon may lead to high lattice thermal conductivity. Also, the phonon DOS distribution shows that the acoustic branches are dominated by the heaviest Ge atoms, and the relatively light S atoms mostly contribute to the optical branches.

Thermal Transport Properties

Next, the thermal transport properties of the GeS_2 monolayer are obtained based on the second- and third-order IFCs. The lattice thermal conductivities in the temperature range of 200–700 K are shown in **Figure 4A**. It shows that the calculated intrinsic κ_l of the isotropic GeS_2 monolayer at 300 K is 9.52 Wm^{-1} K^{-1}, which is larger than those of most well-known 2D TE materials like SnSe (2.02 Wm^{-1} K^{-1}) (Wang et al., 2015), PbTe (2.01 Wm^{-1} K^{-1}) (Zhang et al., 2009), and LaCuOSe (1.73 Wm^{-1} K^{-1}) (Wang et al., 2020), suggesting that its thermal transport properties may not be satisfactory for TE application. In addition, the lattice thermal conductivity of monolayer GeS_2 decreases as temperature increases, typically following a 1/T dependence, which is a common behavior exhibited in the κ_l of crystalline materials and mainly attributed to the intrinsic enhancement in phonon–phonon scattering with temperature (Yang et al., 2016).

To further understand the thermal transport behavior of the GeS_2 monolayer, κ_l is studied using the following formula (Hicks and Dresselhaus, 1993):

$$\kappa_l = \frac{1}{3} C_V V_g l, \tag{3}$$

where C_V, V_g, and l are the lattice heat capacity, phonon group velocity, and phonon mean free path (MFP), respectively. The phonon lifetime and group velocity with respect to frequency are plotted in **Figures 4B, C**. It can be seen that the calculated phonon lifetime is about 1~10^2 *ps* at the range of vibration frequency of acoustic phonons (0~3 THz), which is comparable with rhombohedral GeSe (1~10^2 *ps*) (Yuan et al.,

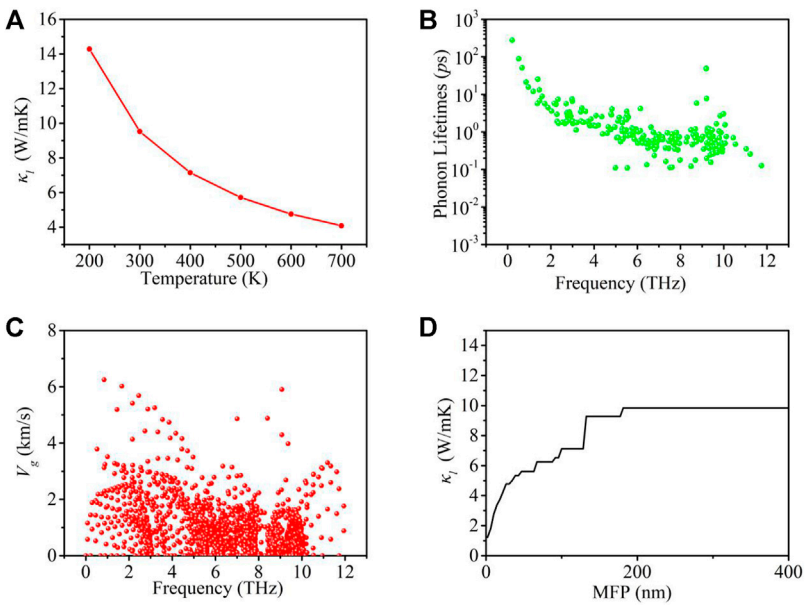

FIGURE 4 | (A) κ_l of monolayer GeS_2. **(B)** Phonon lifetime. **(C)** Phonon group velocity as a function of frequency. **(D)** Cumulative κ_l as a function of the phonon MFP.

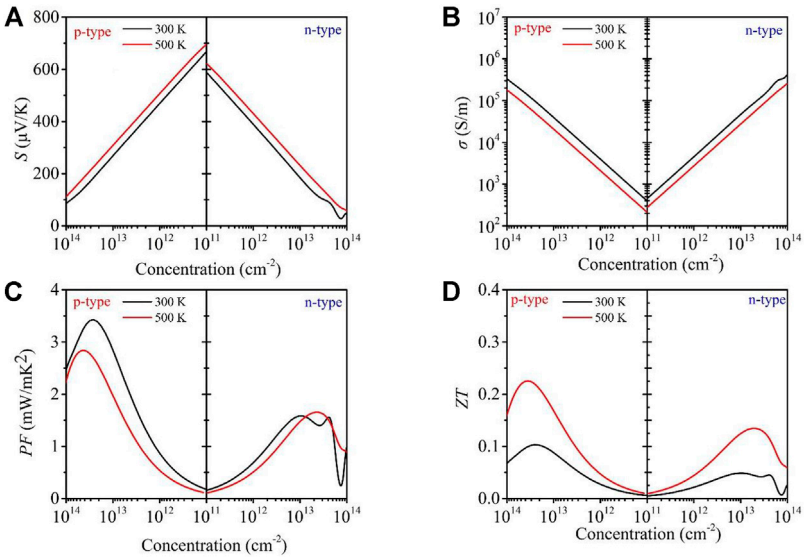

FIGURE 5 | Calculated Seebeck coefficient S **(A)**, electrical conductivity σ **(B)**, power factor *PF* **(C)**, and **(D)** *ZT* values as a function of carrier concentration at different temperatures (300 and 500 K, respectively) for monolayer GeS_2.

2020) and SnP_3 (<10^2 *ps*) (Sun et al., 2020) monolayers. Also, **Figure 4C** shows that the maximum group velocity for the acoustic modes is about 6.2 km/*s*. Then the cumulative κ_l as a function of the MFP for the GeS_2 monolayer is plotted in **Figure 4D**. It is found that the phonon MFP (180 nm) is much larger than those of many materials with high TE performance, such as SnSe (100 nm) (Carrete et al., 2014), SnS (70 nm) (Guo et al., 2015), and PbTe (10 nm) (Tian et al., 2012). The large group velocity and MFP lead to a high lattice thermal conductivity, thus limiting the TE performance of 2D GeS_2.

Electronic Transport Properties

The Seebeck coefficient of the GeS_2 monolayer is given in **Figure 5A**. It is noted that with the carrier concentration increasing from 10^{11} to 10^{14} cm^{-2}, the absolute value of the Seebeck coefficient $|S|$ of *n*- and p-type GeS_2 decreases at the temperatures of 300 and 500 K, which can be explained by the following equation (Guo, Hu et al., 2013):

$$S = \frac{8\pi^2 k_B^2}{3eh^2} m^* T \left(\frac{\pi}{3n}\right)^{2/3}, \tag{4}$$

where k_B, *e*, *h*, m^*, and *n* are the Boltzmann constant, electron charge, Planck constant, effective mass, and carrier concentration, respectively. In addition, it can be seen that the absolute value of the Seebeck coefficient $|S|$ of *n*- and p-type GeS_2 increases as the temperature increases from 300 to 500 K with the carrier concentration at the range of 10^{11}–10^{14} cm^{-2}. Besides, the $|S|$ for p-type GeS_2 is larger than that for *n*-type GeS_2 at a given carrier concentration under 300 and 500 K due to the larger effective mass. For example, the Seebeck coefficient of 696 μV K^{-1} for the p-type system is larger than that of 620 μV K^{-1} for the n-type system along the x-axis at 500 K with a carrier concentration of 1 × 10^{11} cm^{-2}. The $|S|$ is comparable with that of another FeOCl-type monolayer, $Al_2I_2Se_2$, which was reported as a promising TE material (Qi et al., 2021). In addition, the comparison of calculated thermoelectric parameters at 300 K between GeS_2 and $Al_2I_2Se_2$ monolayers has been made in **Table 1**.

The relaxation time, mobility, and effective mass are shown in **Table 2**. Based on the calculated relaxation time, the σ as σ/τ within the constant RTA is obtained, as shown in **Figure 5B**. It can be seen that the σ of both *n*- and p-type systems increases with the increase in carrier concentration at a given temperature, which can be explained with the following formula (Snyder et al., 2020):

$$\sigma = ne\mu, \tag{5}$$

where *n* is the carrier concentration and μ is the mobility of the charge carrier. In addition, σ decreases with the increasing temperature because of more frequent scattering of electrons and lower relaxation time at a higher temperature. As can be clearly noticed, the σ of the n-type system is larger than that of the p-type system due to the larger effective mass for *n*-type GeS_2 at a given temperature and carrier concentration. For example, the value of σ for n-type GeS_2 is 287 S/m, which is larger than that for p-type GeS_2 (210 S/m) at 500 K with a carrier concentration of 1 × 10^{11} cm^{-2}.

The power factor $PF = (S^2\sigma)$ of the GeS_2 monolayer is calculated combined with the Seebeck coefficient and electrical conductivity, as shown in **Figure 5C**. Due to the opposite changes of *S* and σ with the carrier concentration, the *PF* value increases first and then decreases as the carrier concentration increases in all cases. In addition, the *PF* value of p-type GeS_2 is higher than that of *n*-type GeS_2, suggesting that better TE performance can be

TABLE 1 | Comparison of calculated thermoelectric parameters (κ_l, optimal *PF*, and *ZT*) at 300 K between GeS_2 and $Al_2I_2Se_2$ monolayers.

		κ_l	Optimal *PF*	Optimal *ZT*
GeS_2	Our calculation	9.52 W/m K	3.4 mW/m K^2	0.10
$Al_2I_2Se_2$	Other calculation Qi et al. (2021	0.29 W/m K	3.1 mW/m K^2	0.82

TABLE 2 | DP constant E_1, elastic constant *C*, effective mass m^*, carrier mobility μ, and relaxation time τ of the GeS_2 monolayer at room temperature. m_e represents the rest mass of the electron.

	Carrier type	E_1 (eV)	*C* (J m^{-2})	M^* (m_e)	μ (cm^2 $V^{-1}s^{-1}$)	τ (*fs*)
GeS_2	Electron	8.06	87.24	0.83	25.78	12.77
	Hole	7.80	87.24	3.28	1.77	12.52

obtained from the p-type system. The maximum *PF* value occurs at the temperature of 300 K for the p-type system, which is 3.4 mW m^{-1} K^{-2} at the carrier concentration of 2.64 × 10^{13} cm^{-2}. This value is higher than those of other typical TE materials, such as PbTe (3.0 mW m^{-1} K^{-2}) (Pei et al., 2011) and LaCuOSe (2.1 mW m^{-1} K^{-2}) (Wang et al., 2020). Consequently, the prediction of EFF values for electronic transport properties is reliable.

Dimensionless Figure of Merit (*ZT*)

Combining the thermoelectric transport parameters obtained above, the *ZT* values of *n*- and p-type GeS_2 monolayers are estimated, as plotted in **Figure 5D**. It can be found that the maximum *ZT* values for the p-type system are larger than those for the *n*-type system at 300 and 500 K due to the higher *PF* values of p-type GeS_2. At the temperature of 500 K, an optimal *ZT* value of 0.23 for the p-type system can be reached, which is almost twice the value of 0.13 for the *n*-type system. The maximum *ZT* value is smaller than those of most TE materials, like SnSe (2.6 at 923 K) (Zhao et al., 2014) and $GeAs_2$ (2.78 at 800 K) (Wang et al., 2017), suggesting that the TE performance of the GeS_2 monolayer is not as good as the prediction with high-throughput computations indicated, which is attributed to its high lattice thermal conductivity. Therefore, only considering the EFF values without thermal transport properties for predicting the TE performance of materials is incomplete.

CONCLUSION

Motivated by the prediction with high-throughput computations, we systematically study the TE performance of the GeS_2 monolayer *via* first-principles calculations combined with Boltzmann transport theory. Our results show that the electronic transport properties exhibit great performance, consistent with the prediction of high EFF. Specifically, the largest *PF* value of the GeS_2 monolayer reaches 3.4 mW m^{-1} K^{-2} at 300 K because of its high electrical conductivity. However, we also find that its lattice thermal conductivity is as high as 9.52 Wm^{-1} K^{-1} at 300 K, resulting in an unsatisfactory *ZT* value (0.1) for the p-type system. Additionally, the highest *ZT* value is only 0.23 at 500 K. This work suggests that the GeS_2 monolayer is not suitable for TE applications; thus, the prediction of EFF values by high-throughput computations is incomplete.

DATA AVAILABILITY STATEMENT

The original contributions presented in the study are included in the article/Supplementary Material; further inquiries can be directed to the corresponding author.

AUTHOR CONTRIBUTIONS

XW conceived the idea. XW conducted the simulation and analysis. All authors participated in the writing and correction of the manuscript.

ACKNOWLEDGMENTS

We are grateful for the financial support provided by the Education Department of Sichuan Province, China (18ZB0133), the Applied Basic Research Programs of Sichuan Province, China (2018JY0062), and the Research Project of Chengdu University, China (2018XZB17).

REFERENCES

Bardeen, J., and Shockley, W. (1950). Deformation Potentials and Mobilities in Non-polar Crystals. *Phys. Rev.* 80, 72–80. doi:10.1103/physrev.80.72

Bell, L. E. (2008). Cooling, Heating, Generating Power, and Recovering Waste Heat with Thermoelectric Systems. *Science* 321, 1457–1461. doi:10.1126/science.1158899

Biswas, K., He, J., Blum, I. D., Wu, C.-I., Hogan, T. P., Seidman, D. N. D., et al. (2012). High-performance Bulk Thermoelectrics with All-Scale Hierarchical Architectures. *Nature* 489, 414–418. doi:10.1038/nature11439

Carrete, J., Mingo, N., and Curtarolo, S. (2014). Low thermal Conductivity and Triaxial Phononic Anisotropy of SnSe. *Appl. Phys. Lett.* 105, 101907. doi:10.1063/1.4895770

Chen, W., Pöhls, J.-H., Hautier, G., Broberg, D., Bajaj, S., Aydemir, U., et al. (2016). Understanding Thermoelectric Properties from High-Throughput Calculations: Trends, Insights, and Comparisons with experiment. *J. Mater. Chem. C* 4, 4414–4426. doi:10.1039/c5tc04339e

Guo, D., Hu, C., Xi, Y., and Zhang, K. (2013). Strain Effects to Optimize Thermoelectric Properties of Doped Bi2O2Se *via* Tran-Blaha Modified Becke-Johnson Density Functional Theory. *J. Phys. Chem. C* 117, 21597–21602. doi:10.1021/jp4080465

Guo, R., Wang, X., Kuang, Y., and Huang, B. (2015). First-principles Study of Anisotropic Thermoelectric Transport Properties of IV-VI Semiconductor Compounds SnSe and SnS. *Phys. Rev. B* 92, 115202. doi:10.1103/physrevb.92.115202

Heremans, J. P., Jovovic, V., Toberer, E. S., Saramat, A., Kurosaki, K., Charoenphakdee, A., et al. (2008). Enhancement of Thermoelectric Efficiency in PbTe by Distortion of the Electronic Density of States. *Science* 321, 554–557. doi:10.1126/science.1159725

Heyd, J., Scuseria, G. E., and Ernzerhof, M. (2003). Hybrid Functionals Based on a Screened Coulomb Potential. *J. Chem. Phys.* 118, 8207–8215. doi:10.1063/1.1564060

Hicks, L. D., and Dresselhaus, M. S. (1993). Effect of Quantum-Well Structures on the Thermoelectric Figure of merit. *Phys. Rev. B* 47, 12727–12731. doi:10.1103/physrevb.47.12727

Jia, T., Feng, Z., Guo, S., Zhang, X., and Zhang, Y. (2020). Screening Promising Thermoelectric Materials in Binary Chalcogenides through High-Throughput Computations. *ACS Appl. Mater. Inter.* 12, 11852–11864. doi:10.1021/acsami.9b23297

Jonson, M., and Mahan, G. D. (1980). Mott's Formula for the Thermopower and the Wiedemann-Franz Law. *Phys. Rev. B* 21, 4223–4229. doi:10.1103/physrevb.21.4223

Kresse, G., and Furthmüller, J. (1996a). Efficiency of Ab-Initio Total Energy Calculations for Metals and Semiconductors Using a Plane-Wave Basis Set. *Comput. Mater. Sci.* 6, 15–50. doi:10.1016/0927-0256(96)00008-0

Kresse, G., and Furthmüller, J. (1996b). Efficient Iterative Schemes Forab Initiototal-Energy Calculations Using a Plane-Wave Basis Set. *Phys. Rev. B* 54, 11169–11186. doi:10.1103/physrevb.54.11169

Kresse, G., and Hafner, J. (1993). Ab Initiomolecular Dynamics for Liquid Metals. *Phys. Rev. B* 47, 558–561. doi:10.1103/PhysRevB.47.558

Li, W., Carrete, J., A. Katcho, N., and Mingo, N. (2014). ShengBTE: A Solver of the Boltzmann Transport Equation for Phonons. *Comput. Phys. Commun.* 185, 1747–1758. doi:10.1016/j.cpc.2014.02.015

Li, B., Wang, H., Kawakita, Y., Zhang, Q., Feygenson, M., Yu, H. L., et al. (2018). Liquid-like thermal Conduction in Intercalated Layered Crystalline Solids. *Nat. Mater* 17, 226–230. doi:10.1038/s41563-017-0004-2

Li, M., Wang, N., Jiang, M., Xiao, H., Zhang, H., Liu, Z., et al. (2019). Improved Thermoelectric Performance of Bilayer Bi2O2Se by the Band Convergence Approach. *J. Mater. Chem. C* 7, 11029–11039. doi:10.1039/c9tc02188d

Li, R., Li, X., Xi, L., Yang, J., Singh, D. J., and Zhang, W. (2019). High-Throughput Screening for Advanced Thermoelectric Materials: Diamond-Like ABX2 Compounds. *ACS Appl. Mater. Inter.* 11, 24859–24866. doi:10.1021/acsami.9b01196

Liu, W.-S., Zhao, L.-D., Zhang, B.-P., Zhang, H.-L., and Li, J.-F. (2008). Enhanced Thermoelectric Property Originating from Additional Carrier Pocket in Skutterudite Compounds. *Appl. Phys. Lett.* 93, 042109. doi:10.1063/1.2965123

Lucovsky, G., Galeener, F. L., Keezer, R. C., Geils, R. H., and Six, H. A. (1974). Structural Interpretation of the Infrared and Raman Spectra of Glasses in the alloy systemGe1−xSx. *Phys. Rev. B* 10, 5134–5146. doi:10.1103/physrevb.10.5134

Málek, J., and Shánělová, J. (1999). Viscosity of Germanium Sulfide Melts. *J. Non-Crystalline Sol.* 243, 116–122. doi:10.1016/s0022-3093(98)00823-0

Madsen, G. K. H., Carrete, J., and Verstraete, M. J. (2018). BoltzTraP2, a Program for Interpolating Band Structures and Calculating Semi-classical Transport Coefficients. *Comput. Phys. Commun.* 231, 140–145. doi:10.1016/j.cpc.2018.05.010

Miller, S. A., Gorai, P., Aydemir, U., Mason, T. O., Stevanović, V., Toberer, E. S., et al. (2017). SnO as a Potential Oxide Thermoelectric Candidate. *J. Mater. Chem. C* 5, 8854–8861. doi:10.1039/c7tc01623a

Nielsen, M. D., Ozolins, V., and Heremans, J. P. (2013). Lone Pair Electrons Minimize Lattice thermal Conductivity. *Energy Environ. Sci.* 6, 570–578. doi:10.1039/c2ee23391f

Ortiz, B. R., Adamczyk, J. M., Gordiz, K., Braden, T., and Toberer, E. S. (2019). Towards the High-Throughput Synthesis of Bulk Materials: Thermoelectric PbTe-PbSe-SnTe-SnSe Alloys. *Mol. Syst. Des. Eng.* 4, 407–420. doi:10.1039/c8me00073e

Ouyang, T., Jiang, E., Tang, C., Li, J., He, C., and Zhong, J. (2018). Thermal and Thermoelectric Properties of Monolayer Indium Triphosphide (InP3): a First-Principles Study. *J. Mater. Chem. A.* 6, 21532–21541. doi:10.1039/c8ta07012a

Pei, Y., LaLonde, A., Iwanaga, S., and Snyder, G. J. (2011). High Thermoelectric Figure of merit in Heavy Hole Dominated PbTe. *Energ. Environ. Sci.* 4, 2085. doi:10.1039/c0ee00456a

Perdew, J. P., Burke, K., and Ernzerhof, M. (1996). Generalized Gradient Approximation Made Simple. *Phys. Rev. Lett.* 77, 3865–3868. doi:10.1103/physrevlett.77.3865

Petri, I., and Salmon, P. S. (2001). A Neutron Diffraction Study of Glassy GeS2. *J. Non-Crystalline Sol.* 293-295, 169–174. doi:10.1016/s0022-3093(01)00667-6

Qi, H., Sun, Z., Wang, N., Qin, G., Zhang, H., and Shen, C. (2021). Two-dimensional Al2I2Se2: A Promising Anisotropic Thermoelectric Material. *J. Alloys Compd.* 876, 160191. doi:10.1016/j.jallcom.2021.160191

Qiao, L., Zhang, S., Xiao, H. Y., Singh, D. J., Zhang, K. H. L., Liu, Z. J., et al. (2018). Orbital Controlled Band gap Engineering of Tetragonal BiFeO3 for Optoelectronic Applications. *J. Mater. Chem. C* 6, 1239–1247. doi:10.1039/c7tc04160h

Row, D. M., Shukla, V. S., and Savvideset, N. (1981). Phonon Scattering at Grain Boundaries in Heavily Doped fine-grained Silicon-Germanium Alloys. *Nature* 290, 765–766. doi:10.1038/290765a0

Sarikurt, S., Kocabaş, T., and Sevik, C. (2020). High-throughput Computational Screening of 2D Materials for Thermoelectrics. *J. Mater. Chem. A.* 8, 19674–19683. doi:10.1039/d0ta04945j

Shi, H. L., Parker, D., Du, M. H., and Singhet, D. J. (2015). Connecting Thermoelectric Performance and Topological-Insulator Behavior: Bi2Te3 and Bi2Te2Se from First Principles. *Phys. Rev. Appl.* 3, 014004. doi:10.1103/physrevapplied.3.014004

Snyder, G. J., and Toberer, E. S. (2008). Complex Thermoelectric Materials. *Nat. Mater* 7, 105–114. doi:10.1038/nmat2090

Snyder, G. J., Snyder, A. H., Wood, M., Gurunathan, R., Snyder, B. H., and Niu, C. (2020). Weighted Mobility. *Adv. Mater.* 32, 2001537. doi:10.1002/adma.202001537

Sun, G., Kürti, J., Rajczy, P., Kertesz, M., Hafner, J., and Kresse, G. (2003). Performance of the Vienna Ab Initio Simulation Package (VASP) in Chemical Applications. *J. Mol. Struct. Theochem* 624, 37–45. doi:10.1016/s0166-1280(02)00733-9

Sun, Z., Yuan, K., Chang, Z., Bi, S., Zhang, X., and Tang, D. (2020). Ultra-low thermal Conductivity and High Thermoelectric Performance of Two-Dimensional Triphosphides (InP3, GaP3, SbP3 and SnP3): a Comprehensive First-Principles Study. *Nanoscale* 12, 3330–3342. doi:10.1039/c9nr08679j

Tan, G., Zhao, L.-D., and Kanatzidis, M. G. (2016). Rationally Designing High-Performance Bulk Thermoelectric Materials. *Chem. Rev.* 116, 12123–12149. doi:10.1021/acs.chemrev.6b00255

Tang, Y., Gibbs, Z. M., Agapito, L. A., Li, G., Kim, H.-S., Nardelli, M. B., et al. (2015). Convergence of Multi-valley Bands as the Electronic Origin of High Thermoelectric Performance in CoSb3 Skutterudites. *Nat. Mater* 14, 1223–1228. doi:10.1038/nmat4430

Tian, Z., Garg, J., Esfarjani, K., Shiga, T., Shiomi, J., and Chen, G. (2012). Phonon Conduction in PbSe, PbTe, and PbTe1−xSexfrom First-Principles Calculations. *Phys. Rev. B* 85, 184303. doi:10.1103/physrevb.85.184303

Tichý, L., Tříska, A., Barta, Č., Tichá, H., and Frumar, M. (1982). Optical Gaps from 'mean' Bond Energy in Ge1−x S X and Ge K Sb M S N Non-crystalline Solids. *Philosophical Mag. B* 46, 365–376. doi:10.1080/13642818208246447

Togo, A., Oba, F., and Tanaka, I. (2008). First-principles Calculations of the Ferroelastic Transition between Rutile-type andCaCl2-typeSiO2at High Pressures. *Phys. Rev. B* 78, 134106. doi:10.1103/physrevb.78.134106

Wang, Z. L., and Wu, W. (2012). Nanotechnology-Enabled Energy Harvesting for Self-Powered Micro-/Nanosystems. *Angew. Chem. Int. Ed.* 51, 11700–11721. doi:10.1002/anie.201201656

Wang, F. Q., Zhang, S., Yu, J., and Wang, Q. (2015). Thermoelectric Properties of Single-Layered SnSe Sheet. *Nanoscale* 7, 15962–15970. doi:10.1039/c5nr03813h

Wang, X., Wang, Z. L., and Yang, Y. (2016). Hybridized Nanogenerator for Simultaneously Scavenging Mechanical and thermal Energies by Electromagnetic-Triboelectric-Thermoelectric Effects. *Nano Energy* 26, 164–171. doi:10.1016/j.nanoen.2016.05.032

Wang, F. Q., Guo, Y., Wang, Q., Kawazoe, Y., and Jena, P. (2017). Exceptional Thermoelectric Properties of Layered GeAs2. *Chem. Mater.* 29, 9300–9307. doi:10.1021/acs.chemmater.7b03279

Wang, N., Li, M., Xiao, H., Zu, X., and Qiao, L. (2020). Layered LaCuOSe: a Promising Anisotropic Thermoelectric Material. *Phys. Rev. Appl.* 13, 024038. doi:10.1103/physrevapplied.13.024038

Weinstein, B. A., Zallen, R., Slade, M. L., and Mikkelsen, J. C. (1982). Pressure-optical Studies of GeS2glasses and Crystals: Implications for Network Topology. *Phys. Rev. B* 25, 781–792. doi:10.1103/physrevb.25.781

Yang, J., Xi, L., Qiu, W., Wu, L., Shi, X., Chen, L., et al. (2016). On the Tuning of Electrical and thermal Transport in Thermoelectrics: an Integrated Theory-experiment Perspective. *NPJ Comput. Mater.* 2, 15015. doi:10.1038/npjcompumats.2015.15

Yang, Y., Liu, S. C., Wang, X., Li, Z., Zhang, Y., Zhang, G., et al. (2019). Polarization-Sensitive Ultraviolet Photodetection of Anisotropic 2D GeS 2. *Adv. Funct. Mater.* 29, 1900411. doi:10.1002/adfm.201900411

Yuan, J., Cai, Y., Shen, L., Xiao, Y., Ren, J.-C., Wang, A., et al. (2018). One-dimensional Thermoelectrics Induced by Rashba Spin-Orbit Coupling in Two-Dimensional BiSb Monolayer. *Nano Energy* 52, 163–170. doi:10.1016/j.nanoen.2018.07.041

Yuan, K., Sun, Z., Zhang, X., Gong, X., and Tang, D. (2020). A First-Principles Study of the Thermoelectric Properties of Rhombohedral GeSe. *Phys. Chem. Chem. Phys.* 22, 1911–1922. doi:10.1039/c9cp05153h

Zhang, Y., Ke, X. Z., ChenYang, C. F. J., and Kent, P. R. C. (2009). Thermodynamic Properties of PbTe, PbSe, and PbS: First-Principles Study. *Phys. Rev. B.* 80, 024304. doi:10.1103/physrevb.80.024304

Zhang, S., Xiao, H. Y., Peng, S. M., Yang, G. X., Liu, Z. J., Zu, X. T., et al. (2018). Band-Gap Reduction in (BiCrO3)(m)/(BiFeO3)(n) Superlattices: Designing Low-Band-Gap Ferroelectrics. *Phys. Rev. Appl.* 10, 044004. doi:10.1103/physrevapplied.10.044004

Zhao, L.-D., Lo, S.-H., Zhang, Y., Sun, H., Tan, G., Uher, C., et al. (2014). Ultralow thermal Conductivity and High Thermoelectric Figure of merit in SnSe Crystals. *Nature* 508, 373–377. doi:10.1038/nature13184

Conflict of Interest: The authors declare that the research was conducted in the absence of any commercial or financial relationships that could be construed as a potential conflict of interest.